Polymer-Assisted Control of Particle Morphology and Particle Size of Zinc Oxide Precipitated from Aqueous Solution

Andreas Taubert,*[,†,#] Dennis Palms,[†] Özlem Weiss,[§] Maria-Teresa Piccini,[†] and David N. Batchelder[‡]

Max-Planck-Institute for Polymer Research, D-55128 Mainz, Germany, Max-Planck-Institute for Coal Research, D-45470 Mülheim, Germany, and Department of Physics and Astronomy, University of Leeds, Leeds LS2 9JT, U.K.

Received December 4, 2001. Revised Manuscript Received March 29, 2002

Water-soluble poly(ethylene oxide-*block*-methacrylic acid) (P(EO-*b*-MAA)) and poly(ethylene oxide-*block*-styrene sulfonic acid) (P(EO-*b*-SSH)) diblock copolymers were used to control the particle morphologies, sizes and size distributions of zinc oxide precipitated from aqueous solution. With P(EO-*b*-MAA) copolymers, hexagonal prismatic particles form. Their sizes and size distributions depend on the degrees of polymerization of the blocks. With P(EO-*b*-SSH) copolymers, the particle shape reminds one of a "stack of pancakes". These samples have narrow size distributions, regardless of the degrees of polymerization of the P(EO-*b*-SSH) copolymers. All crystals have a central grain boundary assigned to twinning. There is evidence for P(EO-*b*-MAA) copolymer adsorption onto the basal planes of the zinc oxide particles, whereas with P(EO-*b*-SSH) also an adsorption onto the side faces seems possible. The polymers are incorporated to some extent in the crystals and the amount of the polymer incorporated depends on the initial polymer concentration of the reaction solution.

Introduction

Inorganic powders have a wide range of applications as catalysts,[1−3] pigments,[4,5] and fillers,[4] among others. The powder characteristics, i.e., particle shape, size, size distribution, and phase affect the performance of many materials because, e.g., powders containing particles with different habits and a broad size distribution are difficult to process and often lead to low-quality materials. Ceramic slurries of polydisperse and nonuniform powders lead to green bodies with lower sintering densities than samples of monodisperse and uniform particles.[6] Low-density green bodies show significant shrinking and crack formation during the sintering process and poor mechanical stability of the final ceramic.[7] The electronic properties of such ceramics are inferior to ceramics made of monodisperse and uniform powders.[8−10]

Recently, crystallization of inorganic compounds from solution has been extensively studied as a method to obtain well-defined powders that overcome the limitations of poorly defined powders obtained by other processes. Precipitation reactions from aqueous media in particular are a versatile method for the formation of monodisperse and uniform inorganic powders. Many parameters such as temperature, ionic strength or the pH of the reaction solution drastically influence the crystallization process and thus the obtained powders.[11−13]

Inspired by biomineralization,[14,15] many authors have investigated how synthetic polymers affect the crystallization of various minerals.[16−26] These studies found a

* To whom all correspondence should be addressed. Fax +1215 573 2128. E-mail: taubert@seas.upenn.edu.
† Max-Planck-Institute for Polymer Research.
‡ University of Leeds.
§ Max-Planck-Institute for Coal Research.
# Present address: Department of Materials Science and Engineering, 3231 Walnut St., University of Pennsylvania, Philadelphia PA 19104-6272.

(1) Matijevic, E. *Curr. Opin. Colloid Interface Sci.* **1996**, *1*, 176.
(2) Hu, Z.; Chen, S.; Peng, S. *J. Colloid Interface Sci.* **1996**, *182*, 457.
(3) Hölderich, W.; Tjoe *J. Appl. Catal.* **1999**, *184*, 257.
(4) Hollemann, A. F.; Wiberg, N. *Lehrbuch der anorganischen Chemie*, 91st−100th ed.; W. DeGruyter: Berlin, New York, 1985.
(5) West, A. R. *Grundlagen der Festkörperchemie*; VCH: Weinheim, Germany, 1992.
(6) Santos, J. D.; Longo, E.; Leite, R. E.; Varela, J. A. *J. Mater. Res.* **1998**, *13*, 1152.
(7) Tancret, F.; Desgardin, G.; Osterstock, F. *Philos. Mag. A* **1997**, *75*, 505.
(8) Amiji, N.; Tanno, Y.; Okuma, H.; Kann, M. *Adv. Ceram. Mater.* **1986**, *1*, 232.
(9) Bai, S.; Shieh, J.; Tseng, T. *Mater. Chem. Phys.* **1995**, *41*, 104.
(10) Lauf, R. J.; Bond, W. D. *Ceram. Bull.* **1984**, *63*, 278.
(11) Matijevic, E. *Acc. Chem. Res.* **1981**, *14*, 22.
(12) Matijevic, E. *Langmuir* **1986**, *2*, 12.
(13) Matijevic, E. *Chem. Mater.* **1993**, *5*, 412.
(14) Mann, S.; Webb, J.; Williams, R. J. P. *Biomineralization: Chemical and Biochemical Perspectives*; VCH Publishers: Weinheim, Germany, 1989.
(15) Lowenstam, H. E.; Weiner, S. *On Biomineralization*; Oxford University Press: New York, 1989.
(16) Göltner, C. G.; Antonietti, M. *Adv. Mater.* **1997**, *9*, 431.
(17) Cölfen, H.; Antonietti, M. *Langmuir* **1998**, *14*, 582.
(18) Cölfen, H.; Limin, Q. *Chem.—Eur. J.* **2000**, *7*, 106.
(19) Donners, J. J. J. M.; Heywood, B. R.; Meijer, E. W.; Nolte, R. J. M.; Roman, C.; Schenning, A. P. H. J.; Sommerdijk, N. A. J. M. *Chem. Commun.* **2000**, 1937.
(20) Marentette, J. M.; Norwig, J.; Stöckelmann, E.; Meyer, W. H.; Wegner, G. *Adv. Mater.* **1997**, *9*, 647.
(21) Qi, L. M.; Cölfen, H.; Antonietti, M. *Chem. Mater.* **2000**, *12*, 2392.
(22) Öner, M.; Norwig, J.; Meyer, W. H.; Wegner, G. *Chem. Mater.* **1998**, *10*, 460.

10.1021/cm011670m CCC: $22.00
Published on Web 05/02/2002

distinct effect of the additives on particle shapes, sizes, size distributions, and crystal phase. As a result, polymer-controlled precipitation has been used to synthesize monodisperse and uniform inorganic powders and highly ordered nanocomposites.

Although progress has been made in understanding the role of the polymeric additives on nucleation and crystal growth during precipitation, there are still unanswered questions, in particular on the detailed mechanism of nucleation and polymer−surface interactions. There is thus a need to further investigate such precipitation reactions because these experiments will establish a general understanding on how polymers control crystallization on a molecular level. This will in turn open new directions in materials design not only of simple binary compounds but also of more complex inorganic and even organic substances.

Zinc oxide is a convenient model system for controlled crystallization processes, because it has only one crystalline phase, and therefore, polymer-induced phase transitions, which complicate the study, are not observed. Zinc oxide is of technological importance due to its application as a filler material,[4] catalyst,[27−30] and varistor,[10,31] among others. It is thus not only a suitable model system for the investigation of polymer-controlled precipitation but the results presented here and elsewhere may directly be transformed to industrial large-scale synthetic procedures.

Here we demonstrate that water-soluble poly(ethylene oxide-*block*-methacrylic acid) (P(EO-*b*-MAA)) and poly(ethylene oxide-*block*-styrene sulfonic acid) (P(EO-*b*-SSH)) diblock copolymers control particle morphologies, sizes, and size distributions of zinc oxide precipitated from aqueous solution. We also present a simple model of how these polymers influence crystal growth as a function of their chemical composition.

Experimental Section

Materials. The detailed procedure for polymer synthesis is described elsewhere.[32] Precursor polymers were prepared via sequential anionic or a combination of radical and anionic polymerization of *tert*-butyl methacrylate (tBMA) and ethylene oxide (EO). The free methacrylic acid was obtained by treating the P(tBMA-*b*-EO) precursor polymer with an HCl/dioxane mixture at 80 °C for several hours. The polymers obtained via the combined radical−anionic synthesis contain a sulfur atom between the two blocks due to the incorporation of the α,ω-mercaptoethanol initiator. Poly(ethylene oxide-*block*-styrene) precursor polymers were obtained via sequential anionic polymerization of styrene and ethylene oxide.[32] The poly(styrene) blocks were sulfonated with concentrated H_2SO_4 and neutralized with NaOH, yielding poly(ethylene oxide-*b*-styrene sulfonic acid) block copolymers after ion exchange chromatography. The structures of the polymers used in this study are shown in Figure 1.

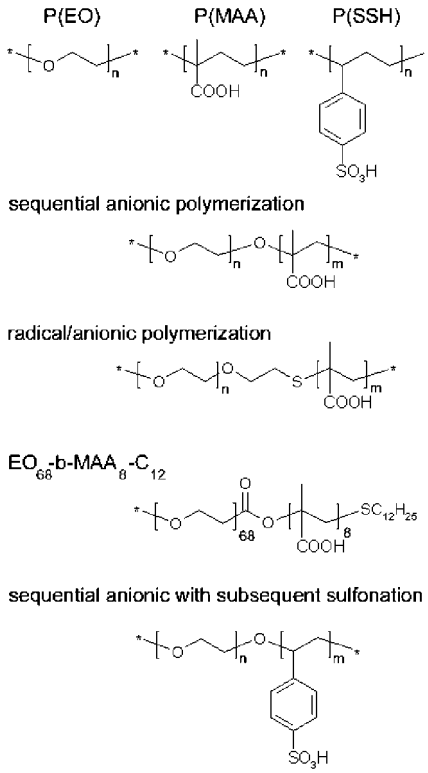

Figure 1. Chemical formulas of the polymers used in this study. The block copolymers are listed according to their synthesis and structure.

In the following, MAA refers to a methacrylic acid, SSH to a styrene sulfonic acid, and EO to an ethylene oxide monomer unit. All subscripts are degrees of polymerization, and C_{12} is a $C_{12}H_{25}$ alkyl chain that is part of one polymer. All other chemicals were of analytical grade and were used without further purification.

Crystallizations. In a typical crystallization, 446 mg of $Zn(NO_3)\cdot 6H_2O$ (Fluka) and 12 mg of a polymer were dissolved in 100 mL of deionized water. The solution was heated to 90 °C and a solution of 210 mg of hexamethylene tetramine (Fluka) in 2 mL of deionized water was added to the slowly stirred solution. The reaction was allowed to proceed for 90 min at 90 °C and terminated by cooling the reaction flask in an ice bath. The white precipitate was separated via centrifugation, washed several times with water and ethanol, and dried in a vacuum oven at 60 °C for 2 days.

Powder X-ray diffraction. Powder X-ray diffraction experiments were made on a Philips PW1820 equipped with a graphite monochromator and proportional counter. The radiation used was Cu K_α (λ = 1.5418 Å), patterns were recorded from 5 to 90°, and the powders were mounted on an aluminum sample holder.

Particle Size Distributions. Particle sizes and distributions were determined from SEM images using Micrografx Designer software. At least 100 crystals were measured per sample. To avoid errors due to projections of the three-dimensional crystal shape to a two-dimensional image, only crystals that were clearly visible and lying flat on the substrate were considered for measurements. The so obtained histograms were fitted using Gauss distributions.[33] Some size distributions can only be reasonably fitted with multipeak distributions. These distributions cannot be analyzed quanti-

(23) Rieger, J.; Thieme, J.; Schmidt, C. *Langmuir* **2000**, *16*, 8300.
(24) Colfen, H. *Macromol. Rapid Commun.* **2001**, *22*, 587.
(25) Qi, L.; Colfen, H.; Antonietti, M.; Li, M.; Hopwood, J. D.; Ashley, A. J.; Mann, S. *Chem.—Eur. J.* **2001**, *7*, 3526.
(26) Bigi, A.; Boanini, E.; Cojazzi, G.; Falini, G.; Panzavolta, S. *Cryst. Growth Des.* **2001**, *1*, 239.
(27) Chinchen, G. C.; Denny, P. J.; Parker, D. G.; Spencer, M. S.; Whan, D. A. *Appl. Catal.* **1987**, *30*, 333.
(28) Himmelfarb, P. B.; Simmons, G. W.; Klier, K.; Herman, R. G. *J. Catal.* **1985**, *93*, 442.
(29) Bowker, M.; Hadden, R. A.; Houghton, H.; Hyland, J. N. K.; Waugh, K. C. *J. Catal.* **1988**, *109*, 263.
(30) Lindsay, R.; Gutierrez-Sosa, A.; Thornton, G.; Ludviksson, A.; Parker, S.; Campbell, C. T. *Surf. Sci.* **1999**, *439*, 131.
(31) Haile, S. M.; Johnson, D. W.; Wiseman, G. H.; Bowen, H. K. *J. Am. Ceram. Soc.* **1989**, *72*, 2004.
(32) Seitz, C. Ph.D. Thesis; University of Mainz: Mainz, Germany, 1999.
(33) Hunter, R. J. *Foundations of Colloid Science*; Oxford Science Publications: Oxford, England 1986; Vol. Vol. 1 + 2.

tatively. To obtain a simpler, though less accurate, relation between the polymer composition and particle size distributions, all distributions were also fitted with a single Gauss curve allowing the identification of very general trends in the data. Data fitting and aspect ratio calculations were done with OriginLab Origin 6.1.

Scanning Electron Microscopy. SEM experiments were performed on dry powders with a LEO 1530 SEM with a field emission gun without sample sputtering. Acceleration voltage was 1 kV, working distance 5 mm, and aperture size 30 μm.

Fluorescence Microscopy. A 20 mg sample of 10−15 μm long zincite crystals[34] were suspended in 5 mL of a 15 mM solution of a fluorescence dye (cresyl violet acetate or fluorescein sodium salt, Fluka) in ethanol and were shaken for several days at room temperature. The powders were separated via centrifugation, washed several times with ethanol and water, and dried at 60 °C in a vacuum oven for 2 days. The dry powders were deposited on a quartz microscopy slide and examined with a Zeiss Axiophot optical microscope with various filters.

Raman Microscopy. The powders were deposited on a piece of aluminum foil and examined in a Renishaw RM1000 Raman microscope equipped with a 50× objective, a CCD camera, and an argon laser (514.5 nm, 4 mW at the sample). The spatial resolution of the microscope, ca. 1 μm, allowed the investigation of single particles.

Thermogravimetric Analysis (TGA) and Thermogravimetry−Mass Spectrometry (TG−MS). TGA experiments were done on a Mettler TG50 from 25 to 900 °C in an oxygen atmosphere. Heating rate was 10 K/min. TG−MS experiments were done on a Netsch STA449C in air and argon. Mass spectra were recorded on a Balzers MS Thermostar coupled to the Netsch 449C. TG−MS experiments were made from 30 to 800 °C at a heating rate of 20 K/min.

Results and Discussion

Particle Morphologies, Sizes, and Size Distributions: Homopolymers. Without additive, polydisperse samples form. They contain large hexagonal prismatic and small thin needlelike crystals (Figure 2a). The changes in particle morphologies, sizes, and size distributions as a function of the polymeric additive will be discussed with respect to this sample, further referred to as the control sample.

The morphologies of the particles precipitated with polymeric additives strongly depend on the chemical nature of the polymers used. These differences are found already at very low polymer concentrations, typically 120 mg/L. (1) With EO_{168}, only large crystals but no thin needles typical for the control samples precipitate (Figure 2b). The crystals have a hexagonal prismatic morphology and are uniform in shape. Crystal faces can easily be distinguished here and no particle aggregation occurs. (2) With MAA_{93}, the sample is polydisperse and no uniform particle shape is observed (Figure 2c). Some particles are rather long and thin and exhibit well-defined crystal faces. Other particles have a roughly spherical shape and are much smaller. The particles often cluster and form aggregates or starlike structures. (3) With SSH_{22}, the hexagonal prismatic habit of the larger crystals in all other samples is not retained. The crystals have a morphology resembling a "stack of pancakes" (Figure 2, parts d and e) without distinct crystal faces. Some particles are spherulitic while others remain rodlike.

(34) Vuin, A. Diploma thesis; Fachhochschule Fresenius Idstein, 1997.

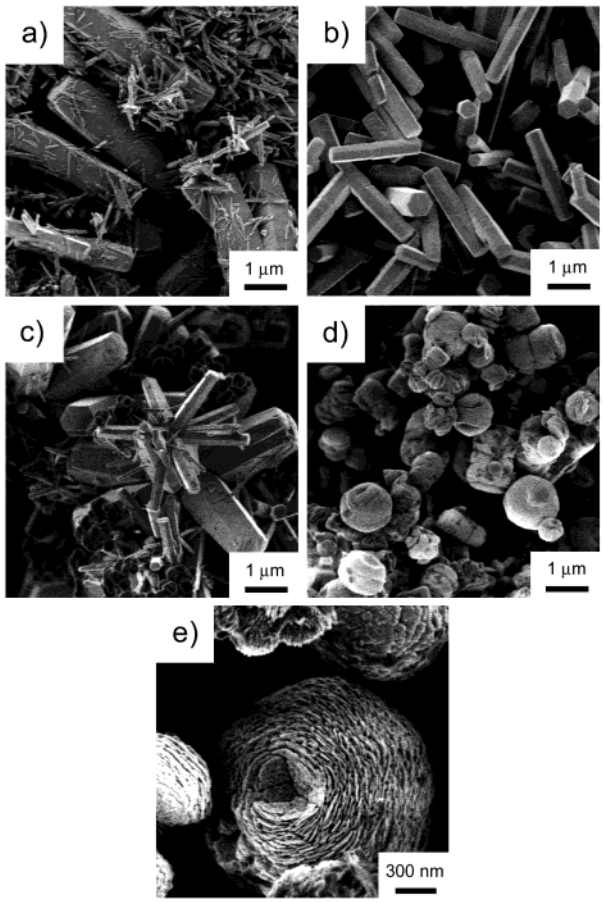

Figure 2. SEM images of (a) a control sample and a series of samples precipitated with 120 mg/L of (b) EO_{168}, (c) MAA_{93}, and (d) SSH_{22}. (e) High magnification image of part d showing the "stack of pancake" morphology.

Some experiments[34] indicated a threshold for the formation of the small needlelike crystals at a polymer concentration of ∼10 mg/L. Since this value is very low, it may be within the statistical error of the experiment and we did not pursue this further. Although the polymers have very different effects on powder formation even at very low concentrations, all powders consisted of zincite as confirmed by powder X-ray diffraction.

The size distributions of the samples in Figure 2 are shown in Figure 3. The control sample has a maximum at very small particle dimensions in both the length and the width distribution. This is because the small needles dominate the contribution of the large crystals to the size distributions. EO_{168} yields crystals with a fairly narrow size distribution and one maximum in the length and in the width that are shifted to larger crystal dimensions compared to the control sample. The sample precipitated with MAA_{93} has similar length and width distributions as the control sample. With SSH_{22}, the size distributions are broad with several maxima. We will now discuss the conclusions drawn from these data.

First, because the length distribution of the control sample is broad, both nucleation and growth must overlap.

Second, the crystals precipitated with MAA_{93} are only about as long as the small crystals in the control sample. Therefore, MAA_{93} must adsorb onto the basal planes of the growing hexagonal crystals and thereby inhibit

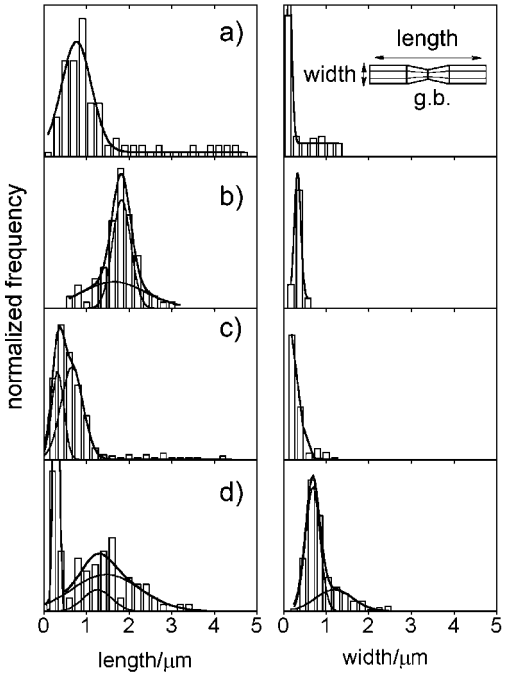

Figure 3. Size distribution histograms of the samples displayed in Figure 1: (a) control sample; (b) 120 mg/L of EO_{168}; (c) 120 mg/L of MAA_{93}; (d) 120 mg/L of SSH_{22}. Inset shows the definition of crystal length *l* and width *w*. g.b. indicates the central grain boundary.

further growth along the long crystal axis. The spherical particles may be crystalline or amorphous; our current study does not answer this question. If they are amorphous, MAA_{93} also stabilizes a noncrystalline precipitate.

Third, the particles precipitated with SSH_{22} exhibit a variety of shapes and sizes. Most of the crystals are approximately rodlike "stack of pancakes" that have a mean length shorter than the length of the large crystals in the control sample. This supports, as with MAA_{93}, the hypothesis that the polyelectrolytes adsorb at the basal planes and inhibit crystal growth in the respective direction. There are however other particles that have approximately the same size as the large crystals in the control sample; this indicates a more complex growth mechanism. The larger mean width of these crystals with respect to the control sample indicates that SSH_{22} also forces the crystals to grow along their short rather than their long axis.

Fourth, the very distinct morphology and size distributions of the particles precipitated with SSH_{22} point to an adsorption of the polymer to the side faces in addition to the adsorption to the basal planes. Polymer adsorption on the side faces will inhibit the formation of hexagonal prisms, the equilibrium morphology of zincite.

Fifth, EO_{168} does not reduce the crystal length or width as dramatically as the polyelectrolytes do compared to the control sample. We therefore conclude that EO_{168} only weakly interacts with the growing crystal. Because uniform crystals with a rather narrow size distribution form here, we infer that this polymer effectively controls crystal nucleation.

Particle Morphologies, Sizes, and Size Distributions: Diblock Copolymers. With all P(EO-*b*-MAA) diblock copolymers, the crystals have a hexagonal

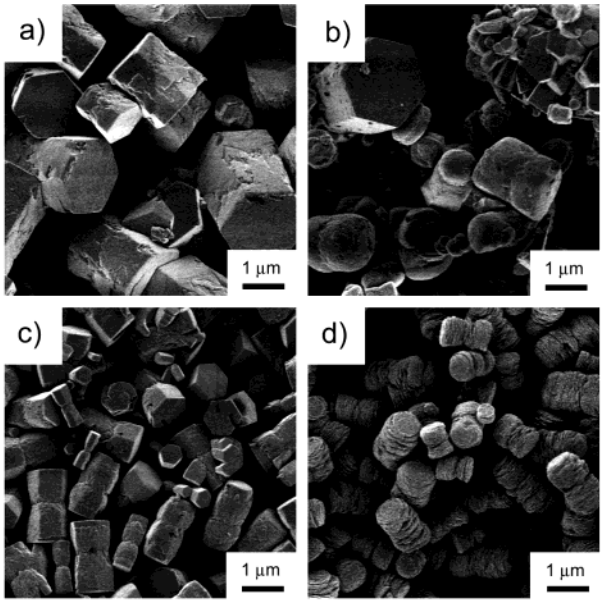

Figure 4. SEM images of a series of zinc oxide powders precipitated with 120 mg/L of (a) EO_{430}-*b*-MAA_{14}, (b) EO_{144}-*b*-MAA_9, (c) EO_{68}-*b*-MAA_8−C_{12}, and (d) EO_{68}-*b*-SSH_{25}.

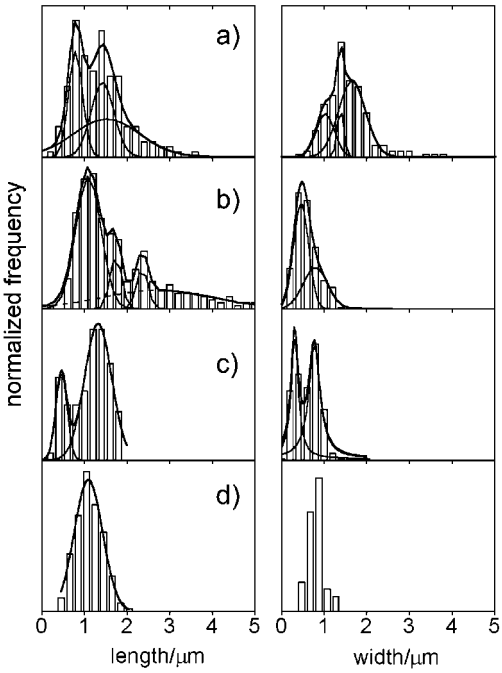

Figure 5. Size distributions of a series of samples crystallized in the presence of 120 mg/L of P(EO-*b*-MAA) and P(EO-*b*-SSH) copolymers: (a) EO_{430}-*b*-MAA_{14}; (b) EO_{67}-*b*-MAA_{13}; (c) EO_{68}-*b*-MAA_8−C_{12}; (d) EO_{68}-*b*-SSH_{25}.

prismatic shape (Figure 4, parts a−c). The crystal sizes, size distributions (Figure 5), and the presence or absence of aggregated prisms such as in Figure 4b top right, however, strongly depend on polymer composition. Only very long P(EO) blocks yield powders of nonaggregated and uniform particles, though with a broad size distribution (Figure 4a). Polymers with shorter EO_n chains ($\sim 90 \leq n \leq \sim 150$ monomer units) lead to samples with an irregular crystal morphology and broad size distribution (Figures 4b and 5b).

With 120 mg/L of EO_{68}-*b*-MAA_8−C_{12}, the crystals are well separated from each other and shorter than the crystals in all other samples precipitated with P(EO-*b*-

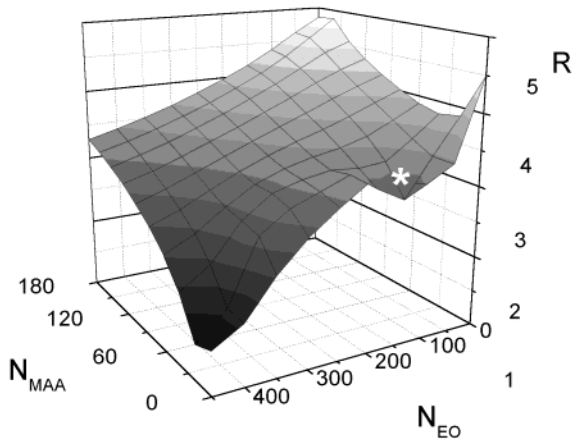

Figure 6. Interpolated aspect ratios **R** of zinc oxide crystals as a function of the degree of polymerization of the poly(ethylene oxide) block (N_{EO}) and the poly(methacrylic acid) block (N_{MAA}).

MAA) copolymers (Figure 4c). They have a narrow, though bimodal size distribution (Figure 5c). The effect of the alkyl chain is also demonstrated in Figure 6. Here, we calculated the expected mean aspect ratios **R** = mean length/mean width of the crystals as a function of the degrees of polymerization of the two blocks by interpolating through the experimentally determined **R**'s. The well marked with an asterisk is the location of EO_{68}-*b*-MAA_8−C_{12} and this deviation off the main interpolated surface clearly demonstrates that the alkyl chain reduces the aspect ratio more than the polymers without an alkyl chain but similar block lengths. Figure 6 also demonstrates that polymers with very long P(EO) blocks and short P(MAA) blocks lead to an overly strong reduction in the aspect ratio.

With P(EO-*b*-SSH) copolymer additives, again "stack of pancake" morphologies form (Figure 4d). The corresponding size distribution (Figure 5d) shows a significant narrowing of both length and width distributions with respect to the P(EO-*b*-MAA) copolymers and the control samples.

The small needles in the control sample form via a secondary nucleation process after ca. 30 min.[35] We will therefore only refer to the large crystals in the control sample to discuss the polymer-controlled growth. With the homopolymers the crystals are almost invariably shorter than the large crystals in the control sample. With diblock copolymers, particle sizes extend up to the same length as in the control sample. The large majority of the crystals however is shorter than the large crystals in the control sample. Because of this, we conclude that the polyelectrolyte blocks preferentially adsorb onto the basal planes of the growing crystals and inhibit further growth along the long crystal axis analogous to the hompolymer case.

Following the same argument as for the homopolymer SSH_{22}, the shape of the particles precipitated with P(EO-*b*-SSH) copolymers indicates that these polymers also adsorb at the side faces of the growing crystals analogous to the SSH_{22} homopolymers. Because the detailed growth mechanism appears to be governed by polymer adsorption, which is controlled by the polymer composition, we will discuss polymer adsorption in the next few paragraphs, followed by a detailed description of proposed growth models.

Table 1. Asymmetry Parameter β of the P(EO-*b*-MAA) Copolymers Used in This Study

N_{EO}	N_{MAA}	β	N_{EO}	N_{MAA}	β
67	13	∼**2.3**	333	21	∼**4**
68	8	∼**2.9**[a]	332	17	∼**4.4**
73	9	∼**2.9**	159	8	∼**4.5**
125	14	∼**3**	430	14	∼**5.5**
144	9	∼**4**			

[a] This polymer contains a $C_{12}H_{25}$ alkyl chain.

Table 2. Asymmetry Parameter β of the P(EO-*b*-SSH) Copolymers Used in This Study

N_{EO}	N_{SSH}	β
38	41	∼**1**
76	43	∼**1.3**
68	25	∼**1.6**

Polymer Adsorption and Proposed Growth Model. Diblock copolymers usually have one block that preferentially adsorbs on a surface (anchor block), whereas the other block remains in solution as a random polymer coil (solution block). The results presented above indicate that the polyelectrolyte blocks act as anchor blocks and the nonionic P(EO) blocks as the solution blocks.

Depending on the relative block lengths, different regimes of adsorption exist for diblock copolymers in a nonselective solvent.[36] With long solution blocks and short anchor blocks, the adsorption limit to a surface is given by the minimum distance that two block copolymers can have from each other before the solution blocks start to interact (solution block regime). The other limiting case is observed with long anchor blocks and short solution blocks. Here, the adsorption limit is given by the minimum distance between two anchor blocks adsorbed on the surface (anchor block regime). Only here, is the surface completely covered by the anchor block.

Marques and Joanny introduced the asymmetry parameter $\beta = (N_S/N_A)^{1/2}$, where N_S is the number of monomer units in the solution block and N_A the number of monomer units in the anchor block.[36] If $\beta > 1$, the adsorption behavior is governed by the solution block, and if $\beta < 1$, it is anchor block controlled. All polymers used in this study exhibit a solution block controlled adsorption (Tables 1 and 2). On the basis of the particle morphologies, sizes, and size distributions as a function of polymer composition, we postulate various adsorption regimes (Figure 7) leading to different growth processes, which we will discuss next.

(1) Without alkyl chains in the P(EO-*b*-MAA) copolymers, crystal growth is controlled by the steric shielding of the P(EO) block toward the solution. EO_{430}-*b*-MAA_{14}, which has the longest P(EO) block and the highest asymmetry parameter (Table 1), provides the best shielding of the growth sites on the crystal surface toward the solution via a large swollen P(EO) coil (Figure 7a). The long solution block also limits the anchor block-to-anchor block distance on the crystal surface at a rather large length scale (the closest solution block-solution block distance is governed by the radius of gyration of the swollen P(EO) block). Free

(35) Taubert, A.; Glasser, G.; Palms, D. *Langmuir*, in press.

(36) Marques, C. M.; Joanny, J. F. *Macromolecules* **1969**, *22*, 1454.

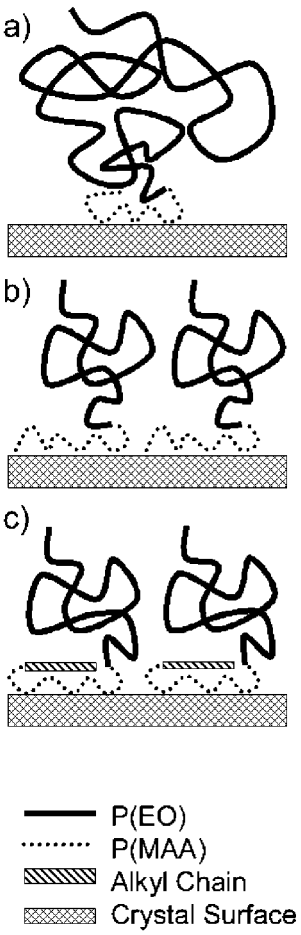

Figure 7. Schematic of postulated adsorption structures. (a) Polymer adsorption with long P(EO) blocks. The crystal surface in the figure can only accommodate one polymer chain and therefore has many free growth sites. (b) Polymer adsorption with shorter P(EO) blocks. The crystal surface in the figure can accommodate two polymers. Less growth sites are free and growth therefore is more perturbed than in a). The steric shielding toward the solution is less distinct. (c) C_{12} chain in close proximity to the crystal surface and preventing rapid diffusion of Zn^{2+} to the surface, which leads to a slow and well-controlled crystal growth.

surface sites are available for growth once Zn^{2+} ions have reached the surface. Growth is probably not limited by incorporation of Zn^{2+} to the crystal, but rather by the transport to the crystal surface through the swollen P(EO) block.

(2) With shorter P(EO) blocks, the steric shielding is less distinct (Figure 7b). The shorter solution blocks also allow for shorter mean anchor block-to-anchor block distances on the crystal surfaces, which reduces the number of undisturbed growth sites available and forces the formation of crystals like in Figure 3b top right. This leads to a somewhat uncontrolled crystal growth as in the case of EO_{144}-*b*-MAA_9.

(3) The presence of an alkyl chain in EO_{68}-*b*-MAA_8−C_{12} improves the shielding of the crystal surface covered with the adsorbed polymer toward the solution (Figure 7c). Because the *hydrophobic* C_{12} chain is directly connected to the poly(methacrylic acid) block adsorbed on the crystal surface, this polymer yields a crystal surface covered with a hydrophobic rather than a hydrophilic polymer layer. This presumably slows down the diffusion of Zn^{2+} to the surface of the growing crystal and allows for a well-defined growth process because the Zn^{2+} delivery to the growth sites is slower than without the alkyl chain.

(4) With P(EO-*b*-SSH) copolymers, the length of the solution block plays a less significant role, presumably due to a better shielding of surface sites by the benzene rings of the P(SSH) block. These polymers also adsorb at the side faces and inhibit the formation of the hexagonal prismatic equilibrium morphology. It is currently not clear why this happens. As a result of our data, however, we may speculate that that a long P(EO) block, an alkyl chain, or a P(SSH) block is necessary for the formation of uniform crystals.

It should be stressed at this point that these scenarios are based only on the final morphologies and size distributions of the samples, but they are further supported by kinetic experiments.[35] Polymer adsorption on the basal planes may be explained with electrostatic interactions between the polyelectrolyte blocks and the polar basal planes. We may also speculate that the geometry, the size, or the acid strength of the poly(methacrylic acid) prevents polymer adsorption on the less polar side faces. Further experiments will be necessary to address the effect of these copolymers on an atomic length scale.

Central Grain Boundary. The presence of a central grain boundary in most crystals indicates twinning. Zinc oxide has a polar lattice and the (0001) and the (000$\bar{1}$) faces have opposite surface charges.[5] Consequently, the basal planes of a twinned particle should have *identical* surface charges. In this case, we expect identical adsorption of ionic molecules onto the basal planes (Figure 8a). On the other hand, if the central grain boundary is *not* due to twinning, we expect a different adsorption behavior of charged molecules to the basal planes because a negatively charged molecule will not adsorb to a negatively charged crystal surface and vice versa.

We used charged fluorescence dyes to investigate the adsorption and found equally high fluorescence intensities at both ends and a low intensity at the side faces of the crystals (Figure 8b). As a result, we conclude that both basal planes have the same surface charge. This automatically implies that twin formation and a polarity inversion occur at the central grain boundary. This is consistent with recent results by Klap et al.[37] who found a similar central grain boundary in $AlPO_4$-5 crystals. They show that the crystal lattice on both sides of the grain boundary has an 180° reversed polarity consistent with two crystal domains with different orientation separated by the grain boundary.

Polymer Incorporation. We used TGA and TG−MS to investigate polymer incorporation in the crystals. The control sample loses ca. 1−2 wt % due to water desorption, as detected from the corresponding mass spectra. With an EO_{68}-*b*-MAA_8−C_{12} solution concentration of 120 mg/L ca. 4% and with 3 g/L^{-1} ca. 30% weight losses are found. The weight loss with 120 mg/L EO_{68}-*b*-SSH_{25} is ca. 8%. The molecular weight of EO_{68}-*b*-SSH_{25} is approximately twice the molecular weight of EO_{68}-*b*-MAA_8−C_{12}. Consequently, the molar polymer concentration in the crystals is about equal in these two samples. Mass spectroscopy finds C_2 and C_3 fragments

(37) Klap, G. J.; Wübbenhorst, M.; Jansen, J. C.; van Koningsveld, H.; van Bekum, H.; van Turnhout, J. *Chem. Mater.* **1999**, *11*, 3497.

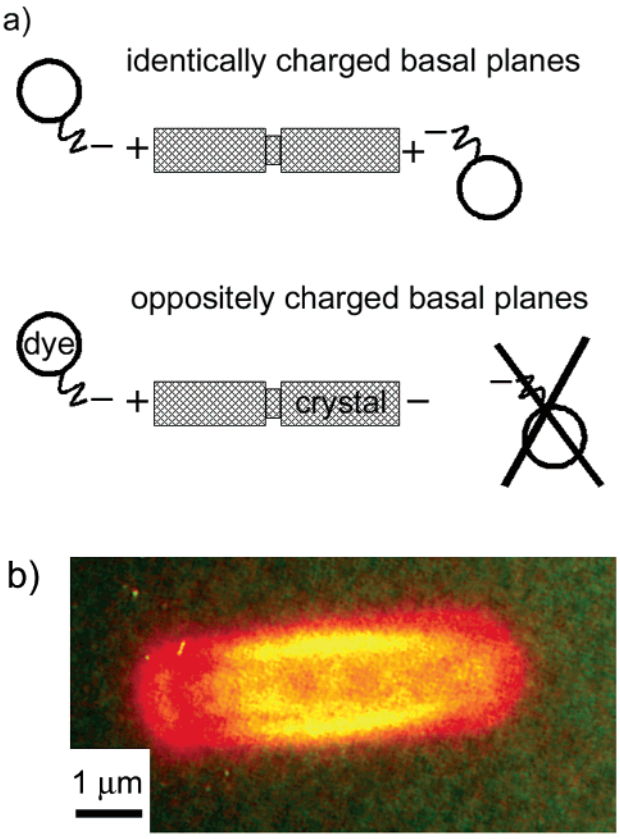

Figure 8. (a) Schematic of the zinc oxide crystal with adsorbed dyes. If the crystal is a twin, both basal planes will have identically charged basal planes and hence dyes will adsorb at both basal planes to the same extent. If the crystal is an untwinned entity, the basal planes will be oppositely charged and the dyes will adsorb to different extents. (b) Fluorescence microscopy image of a sample of large crystals treated with a solution of cresyl violet acetate. The image shows equally high fluorescence intensities at both basal planes (red). The yellow color at the side faces is due to scattered light.

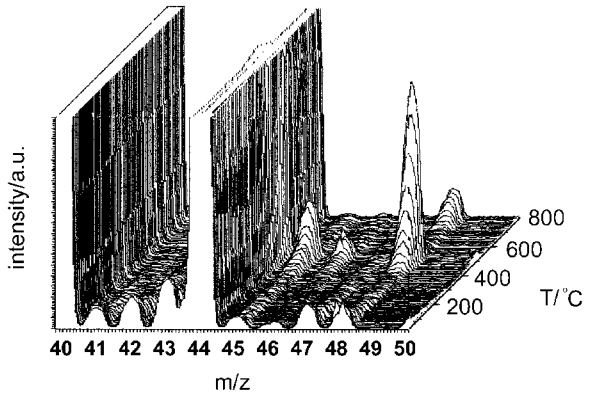

Figure 9. Typical mass spectra obtained from a sample crystallized with 120 mg/L EO_{68}-*b*-SSH_{25} vs heating temperature: *m*/*z* 40, $C_3H_2^+$; *m*/*z* 41, $C_3H_3^+$; *m*/*z* 42, $C_3H_4^+$; *m*/*z* 43, $C_3H_5^+$; *m*/*z* 44 and 45, CO_2^+; *m*/*z* 46 and 47, NO_2^+; *m*/*z* 48, SO^+.

along with CO_2 and water. With EO_{68}-*b*-SSH_{25}, the mass spectra (Figure 9) also shows SO.

The weight loss in all samples is thus due to polymer and water. TGA and TG−MS thus confirm that at higher concentration more polymer is closely associated with the crystals, either by adsorption or incorporation. The high temperatures at which the weight losses occur

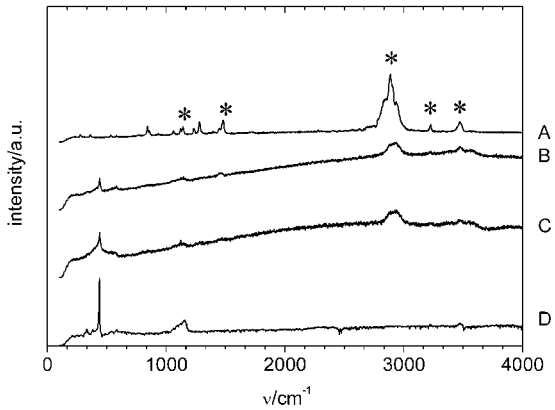

Figure 10. Raman spectra of an EO_{68}-*b*-MAA_8−C_{12} copolymer (A) and of technical zincite (Fluka) (D) along with the Raman spectra of a sample that was crystallized with 120 mg/L EO_{68}-*b*-MAA_8−C_{12} before (C) and after (B) plasma treatment. Asterisks denote Raman bands of the polymer that are visible in the Raman spectra of the precipitate.

indicate that the polymer is stabilized within a matrix; i.e., it is located *in* the crystal and not on the surface.

Polymer *incorporation* was investigated using Raman microscopy. To that end, we acquired Raman spectra from EO_{68}-*b*-SSH_{25}, a technical zincite powder without any organic component, and a sample precipitated with EO_{68}-*b*-SSH_{25} (Figure 10). The precipitate was treated with an O_2/Ar plasma to remove surface contaminations such as adsorbed EO_{68}-*b*-SSH_{25} and subsequently re-examined.

The zincite bands are in good agreement with reported values.[38−40] The perturbation of the Raman spectra of the polymer by the crystallization process suggests that the polymer is incorporated into the zincite matrix. In addition, the Raman spectra of the plasma-treated samples show both polymer and zincite bands with intensities similar to those of the freshly precipitated samples. The continued presence of the polymer bands in the Raman spectra after plasma treatment of the sample provides further evidence that the polymer is incorporated in the crystals. The fact that the Raman bands of the polymer in the powders are intense even after plasma treatment is an indication that a rather large volume fraction (∼30 vol %, as calculated from the area of the respective bands) of the powders are occupied by incorporated polymer. The high amount of incorporated polymer is responsible for distinct variations in the internal structure of the particles, as will be discussed in a forthcoming paper.[41]

Acknowledgment. Thanks are due to Prof. G. Wegner for helpful discussions, Dr. C. Seitz and Dr. D. J. Valenti for polymer synthesis, A. Vuin for the synthesis of the large crystals, E. Muth for TGA, and G. Glasser for SEM experiments. Renishaw GmbH is thanked for the loan of the Raman microscope. D.N.B. thanks the Max-Planck-Institute for Polymer Research for its support and hospitality during his visit to Mainz.

(38) Arguello, C. A.; Rousseau, C.; Porto, S. P. S. *Phys. Rev.* **1969**, *181*, 1351.
(39) Calleja, J. M.; Cardona, M. *Phys. Rev. B* **1977**, *16*, 3753.
(40) Damen, T. C.; Porto, S. P. S.; Tell, B. *Phys. Rev.* **1966**, *142*, 570.
(41) Taubert, A.; Kübel, C.; Martin, D. C. *J. Phys. Chem. B*, submitted.

This work was funded by the Federal Ministry of Research and Technology, Grant No. 03D0045.

Supporting Information Available: Tables listing the polymers used in this study and the particle size data. This material is available free of charge via the Internet at http://pubs.acs.org.

CM011670M